

Quasiparticle and fully self-consistent GW methods: an unbiased analysis using Gaussian orbitals

Gaurav Harsha,¹ Vibin Abraham,¹ Ming Wen,¹ and Dominika Zgid^{1,2}

¹*Department of Chemistry, University of Michigan, Ann Arbor, Michigan 48109, USA*

²*Department of Physics, University of Michigan, Ann Arbor, Michigan 48109, USA*

We present a comparison of various approximations to self-consistency in the GW method, including the one-shot G_0W_0 method, different quasiparticle self-consistency schemes, and the fully self-consistent GW (sc GW) approach. To ensure an unbiased and equitable comparison, we have implemented all the schemes with the same underlying Matsubara formalism, while employing Gaussian orbitals to describe the system. Aiming to assess and compare different GW schemes, we analyze band gaps in semiconductors and insulators, as well as ionization potentials in molecules. Our findings reveal that for solids, the different self-consistency schemes perform very similarly. However, for molecules, full self-consistency outperforms all other approximations, i.e., the one-shot and quasiparticle self-consistency GW schemes. Our work highlights the importance of implementation details when comparing different GW methods. By employing state-of-the-art fully self-consistent, finite temperature GW calculations, we have successfully addressed discrepancies in the existing literature regarding its performance. Our results also indicate that when stringent thresholds are imposed, the sc GW method consistently yields accurate results.

I. INTRODUCTION

The GW approximation [1–4] is ubiquitously used in chemistry and physics to study correlated quantum many-body systems beyond the mean-field methods such as the density functional theory [5, 6] (DFT) and Hartree-Fock (HF). GW is one of the simplest in a series of systematically improvable approximations to Hedin’s formulation of the many-body perturbation theory [1], in which the self-energy is approximated as the product of single-particle Green’s function G and the screened Coulomb interaction W . It has proven to be fairly accurate in describing photo-electron spectra in both finite [7–16] and extended systems [17–24], and is also considered as an ideal starting point for sophisticated quantum embedding theories such as dynamical mean-field theory [25–30] and self-energy embedding theory [31–34]. The success of GW can be attributed to its ability to accurately describe the screening of Coulomb interaction between electrons in contrast to fully iterative methods such as self-consistent second order (GF2) [35] based on the diagrammatic expansion with bare Coulomb interactions. Moreover, GW also accounts for electron exchange, albeit at the lowest order, i.e., using the Fock diagram. Diagrammatic similarities between GW and other accurate methods such as coupled cluster (CC) and random phase approximation (RPA) are also well known, which further explain its accuracy [36–39].

The formal computational scaling of GW equations is $\mathcal{O}(N^6)$, where N is a measure of the system size. After approximations such as the decomposition of two-electron integrals [40–42], this scaling is brought down to $\mathcal{O}(N^4)$ making GW an attractive method to study large, realistic systems. By using tensor hyper-contraction techniques, this computational scaling can be reduced even further to $\mathcal{O}(N^3)$ [43].

Despite the low computational scaling, storing and manipulating dynamical quantities such as the Green’s function and the self-energy can still become costly. As a result, early implementations [44–46] of the GW method relied on numerous approximations, e.g., plasmon-pole models for the dielectric function [47, 48], in addition to the usual ones, such as the use of pseudopotentials and finite basis-sets for electronic orbitals. The notion of one-shot GW (or G_0W_0), where just a single iteration of GW is performed, was also introduced. The diagonal approximation is another one that is now commonly used with G_0W_0 , in which corrections are introduced only for the quasiparticle energies while eigenvectors of the initial mean-field calculation are retained. This results in a self-energy with no off-diagonal terms (in the basis of mean-field eigenvectors).

It is clear that performing only a single iteration of GW leads to results that depend strongly on the mean-field starting point. However, with sufficient experience, an optimal reference for G_0W_0 can sometimes be found [49, 50]. For example, in semiconductors and insulators, G_0W_0 based on DFT calculations with local density approximation (LDA) or Perdew-Becke-Ernzerhof [51] (PBE) functional provides accurate band gaps [2, 52–57], while for molecules, G_0W_0 with hybrid DFT reference, containing some level of exact exchange, provides accurate ionization potentials (IP) [9, 15, 16, 58–60]. In fact, such a G_0W_0 description can be tuned to perform better than full self-consistency.

As algorithmic and computational capabilities improved over time, implementations of fully self-consistent solution of GW equations, called as sc GW , have become more common [7, 8, 17, 18, 22, 61–66]. Self-consistency guarantees black-box results, independent of the mean-field reference. Moreover, at self-consistency, the GW approximation is derivable from the Luttinger-Ward functional [67–69] and, therefore, ensures that thermodynamic variables such as total energy, entropy,

grand-potential, etc., are well defined, i.e., different ways of calculating these quantities yield identical results.

In the pursuit of combining the merits of scGW and G_0W_0 , two notable methodologies for quasiparticle self-consistent GW have emerged [70–73]. The first approach by van Schilfgaarde et al. [70, 71], hereafter referred as qpGW-I, involves the construction of an effective, static (or frequency-independent) exchange-correlation potential from the dynamical (or frequency-dependent) self-energy in each iteration of the GW cycle. This effective potential is then used to solve the quasiparticle equation yielding a new Green’s function for the next iteration. Another approach by Kutepov et al. [72], referred here as qpGW-II, proposes a first-order linear-in-frequency approximation to the self-energy. Through further manipulations, an effective Hamiltonian is derived, with its eigenvalues corresponding to quasiparticle energies. Schematic diagrams summarizing the quasiparticle self-consistency schemes and scGW are shown in Fig. 1.

Both forms of quasiparticle self-consistency, qpGW-I and qpGW-II, have been shown to be reasonably accurate both for band gaps in semiconductors [17, 72, 74], as well for ionization potential in molecules [11]. By their construction, they also remedy the problem of mean-field-dependence present in G_0W_0 . Several other ways to marry the benefits of G_0W_0 and scGW have also been proposed, e.g., partial self-consistency in G_0W_0 [61, 75], eigenvalue self-consistent GW (evGW) [76], etc., most of which only partially cure the reference-dependence. For the purpose of this paper, we will focus on one-shot, quasiparticle, and fully self-consistent GW methods.

A straightforward comparison of new approximations, such as quasiparticle self-consistency, in GW with existing methodologies of G_0W_0 and particularly scGW is difficult and presents several challenges. First, accurate implementations of scGW have become possible only recently. The issue is further complicated by the fact that each GW implementation varies in several technical aspects. These include, but are not limited to, the choice of single-particle basis, whether finite-temperature or zero-temperature formalism is employed, and accuracy of grids for time- and frequency-representation of Green’s function and self-energy. Furthermore, when finite-temperature formalism is employed, analytical continuation (AC) of the results from Matsubara to the real frequency axis becomes necessary. This compels another decision in selecting an appropriate AC method from among many alternatives [77–81]. Rigorous comparisons of different quasiparticle and full self-consistency schemes in GW have therefore been rare [11, 21, 22, 62, 82].

Grumet et al. conducted a comparative analysis of different self-consistency schemes in GW, as outlined in Ref. 22. Their study revealed that fully self-consistent GW, performed on the imaginary-time grid, yielded larger band gaps compared to the fully self-consistent

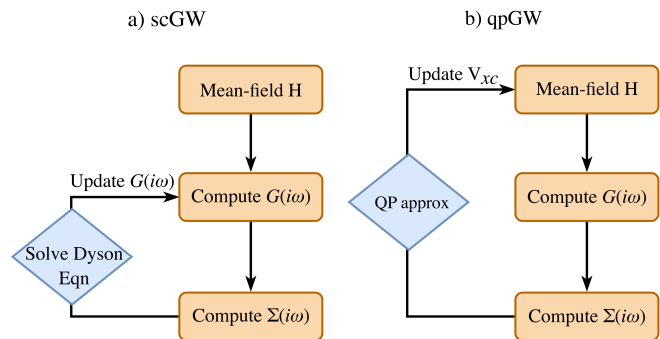


FIG. 1. Schematic representation of different self-consistency schemes in the GW approximation. The central object in scGW is the correlated Green’s function G , whereas in qpGW, it is the effective mean-field Hamiltonian.

GW reported by Kutepov [83]. Additionally, the band gaps obtained using the scGW approach by Kutepov were notably larger than those from the qpGW-I scheme reported by Shilfgaarde-Kotani-Faleev [17, 71], which was also included for comparison purposes in Grumet’s work. Consequently, an unbiased determination of whether quasiparticle self-consistent GW results closely resemble scGW, as reported by Kutepov, or if there is a difference between scGW and qpGW-I, as reported by Grumet et al., was not feasible based on their findings. Even for molecules, the ambiguity in the relative accuracy of qpGW-I and scGW persists. While Koval and co-authors [62] reported that scGW provides better IPs as compared to qpGW-I, similar study by Caruso et al. [11] suggested otherwise. Meanwhile, the application and analysis of qpGW-II for molecules remain completely unexplored.

Our study aims to resolve this discrepancy by implementing and comparing G_0W_0 , qpGW-I, qpGW-II, and scGW methods, all within the framework of Matsubara Green’s functions as explored in Ref. 66. By maintaining identical underlying implementation details across the various methods, we ensure a fair and unbiased comparison. Furthermore, our implementations utilize Gaussian orbitals as the one-particle basis, eliminating such bias as is present when methods implemented employing different one-particle bases, e.g., linearized augmented-plane-wave (LAPW) or plane wave basis, are compared against each other. To differentiate between G_0W_0 , qpGW-I, qpGW-II, and scGW methods, we examine band gaps in selected semiconductors and insulators, as well as ionization potentials in selected molecules. We also compare trends and potential issues that arise in the convergence of self-consistent schemes. While other studies comparing different approximations in the GW method have been conducted in the literature, e.g., in Refs. [11, 84, 85], they either utilize different implementations for scGW and qpGW, or lack a direct comparison between the two methods.

II. THEORY

We first describe the theoretical details for the various *GW* methodologies that we implement and compare in this paper. In the finite-temperature Matsubara formalism employed here, the equilibrium single-particle Green's function on the imaginary-time axis is defined as

$$G_{ij}(\tau) = -\frac{1}{\mathcal{Z}} \text{Tr} \left[e^{-(\beta-\tau)(H-\mu N)} c_i e^{-\tau(H-\mu N)} c_j^\dagger \right], \quad (1)$$

where $\tau \in [0, \beta)$ is the imaginary time, H and N are the Hamiltonian and number operators, respectively, μ is the chemical potential, and operators c_i (c_i^\dagger) annihilate (create) a particle in the i th spin-orbital. Finally, the partition function \mathcal{Z} is defined as

$$\mathcal{Z} = \text{Tr} \left[e^{-\beta(H-\mu N)} \right], \quad (2)$$

where $\beta = 1/k_B T$ is the inverse temperature. The Fourier transform between the imaginary-time and the Matsubara Green's function is defined as

$$G_{ij}(i\omega_n) = \int_0^\beta d\tau G_{ij}(\tau) e^{i\omega_n \tau}, \quad (3a)$$

$$G_{ij}(\tau) = \frac{1}{\beta} \sum_n G_{ij}(i\omega_n) e^{-i\omega_n \tau}. \quad (3b)$$

The fermionic Matsubara frequencies take the values $\omega_n = (2n+1)\pi/\beta$, where $n = 0, \pm 1, \pm 2, \dots$ and so forth. Further, we use a general two-body electronic Hamiltonian, written as

$$H = \sum_{ij} (H_0)_{ij} c_i^\dagger c_j + \frac{1}{2} \sum_{ijkl} U_{ijkl} c_i^\dagger c_k^\dagger c_l c_j, \quad (4)$$

where the one-electron integrals H_0 describe the kinetic energy and the interaction of electrons with the nuclei and other external potential, while the two-electron integrals U describe the Coulomb repulsion between electrons. Generalizations of this Hamiltonian to the case of periodic / extended systems are straightforward. For an explicit notation and equations, the reader may refer to Ref. 66. We should note that in all the discussion below, unless stated otherwise, we consider all the quantities, such as the Hamiltonian, Green's function, self-energy, etc. in the non-orthogonal atomic-orbital (AO) basis.

A. The *GW* approximation

Hedin's formulation of the many-body perturbation theory describes a coupled set of equations for the interacting single-particle Green's function G , the vertex function Γ , the irreducible polarization Π , the screened Coulomb interaction W , and the self-energy Σ of a system.

In the simplest non-trivial approximation, higher order corrections to the vertex function are ignored, i.e., Γ is defined as a Dirac-delta function. As a result, the polarization Π and the effective screened Coulomb interaction W are given by

$$\Pi_{abcd}(\tau) = G_{da}(\tau) G_{bc}(-\tau), \quad (5a)$$

$$W_{ijkl}(i\Omega_n) = U_{ijkl} + \sum_{abcd} U_{ijab} \Pi_{abcd}(i\Omega_n) W_{cdkl}(i\Omega_n), \quad (5b)$$

where $\Omega_n = 2n\pi/\beta$ are the bosonic Matsubara frequencies with $n = 0, \pm 1, \pm 2, \dots$. Subsequently, the total *GW* self-energy is expressed as a sum of static and dynamical terms, i.e.,

$$\Sigma_{\text{total}}(\tau) = \Sigma_\infty + \Sigma(\tau), \quad (6a)$$

$$\Sigma_{\infty,ij} = \sum_{ab} \rho_{ab} (U_{ijba} - U_{iabj}), \quad (6b)$$

$$\Sigma_{ij}(\tau) = - \sum_{ab} G_{ab}(\tau) \tilde{W}_{iabj}(\tau), \quad (6c)$$

where the static self-energy Σ_∞ arises from the contraction of density matrix $\rho = -G(\tau = \beta^-)$ with the bare Coulomb interaction U and contains the Hartree-Fock diagrams, while the dynamical contribution comes from the effective screened Coulomb interaction \tilde{W} defined as

$$\tilde{W}(\tau) \xleftrightarrow[\text{Transform}]{\text{Fourier}} \tilde{W}(i\Omega_n) = W(i\Omega_n) - U. \quad (7)$$

Finally, the full correlated Green's function is defined as

$$[\mathbf{G}^{-1}](i\omega_n) = [\mathbf{G}_0^{-1}](i\omega_n) - \mathbf{\Sigma}(i\omega_n), \quad (8a)$$

$$[\mathbf{G}_0^{-1}](i\omega_n) = (i\omega_n + \mu) \mathbf{S} - \mathbf{F} \quad (8b)$$

where \mathbf{S} denotes the overlap matrix, $\mathbf{\Sigma}(i\omega_n)$ is the Fourier transform of $\Sigma_{ij}(\tau)$, and $\mathbf{F} = \mathbf{H}_0 + \mathbf{\Sigma}_\infty$ is a Fock matrix.

1. Self-consistent *GW*

In sc*GW*, Eqs. (5) to (8) are solved in an iterative manner until self-consistency is achieved. Numerically, convergence means that updates from the subsequent iterations to the quantities involved, such as G and Σ or derived properties such as total energy, are smaller than a specified threshold. We initialize each calculation with $\Sigma_\infty^{(0)} = V_{\text{eff}}$ and $\Sigma^{(0)}(\tau) = 0$, where V_{eff} represents the effective Hartree and exchange potential obtained from the initial mean-field calculation. This defines the initial Green's function through Eq. (8a). Following that, the algorithm used for sc*GW* in this work can be succinctly described as:

1. At the n th iteration, use the Green's function $\mathbf{G}^{(n)}$ to build the static and dynamical parts of the

self-energy $\Sigma^{(n)}$. Note that the dynamical self-energy $\Sigma(\tau)$ is first constructed on the imaginary time axis, and then transformed to the Matsubara frequency axis using Eq. (3).

2. The new Green's function $\mathbf{G}^{(n+1)}$ is computed by substituting $\Sigma^{(n)}$ in Eq. (8a), an equivalent of the Dyson equation. The chemical potential is fixed by ensuring the correct particle number in the associated one-particle density matrix,

$$\rho^{(n+1)} = -\mathbf{G}^{(n+1)}(\tau = \beta^-). \quad (9)$$

3. Calculate the one- and two-body contributions to the total energy,

$$E_{\text{Total}} = E_{\text{nuclear}} + E_1 + E_2, \quad (10a)$$

$$E_1 = \frac{1}{2} \text{Tr} [\rho (\mathbf{H}_0 + \mathbf{F})], \quad (10b)$$

$$E_2 = \sum_{n=-\infty}^{\infty} \text{Tr} [\mathbf{G}(i\omega_n) \Sigma(i\omega_n)]. \quad (10c)$$

Here, E_1 represents the Hartree-Fock contribution, while E_2 incorporates dynamical correlation through the Galitskii-Migdal formula [86, 87]. We consider the self-consistent loop to be converged if the change in both the one-particle and total energy in the current iteration, compared with the previous one, is smaller than specified threshold. Otherwise, we repeat steps 2-5.

In all the scGW calculations presented here, the relative fluctuation in particle number is enforced to be less than 10^{-8} . Meanwhile, an absolute threshold of 10^{-6} a.u. is used as the convergence criterion of total energies.

2. One-shot GW

The premise of one-shot GW is that the reference mean-field calculation serves as a very good starting point. While this assumption may be reasonably accurate for some weakly correlated systems, in general, it introduces a strong dependence of the G_0W_0 results on the mean-field reference. Following common practice in G_0W_0 , we also employ the diagonal approximation here. Our G_0W_0 calculations can be described with the following steps:

1. Starting with the same initial Green's function G_0 as in scGW, we construct the dynamical part of the self-energy Σ on the imaginary axis. In particular, we are only interested in $\Sigma_{ii}(i\omega_n) = \langle \psi_i | \Sigma(i\omega_n) | \psi_i \rangle$, where $|\psi_i\rangle$ is the i th eigenvector of the mean-field Fock matrix $\mathbf{F}^{(0)}$ with the eigenvalue ϵ_i^0 .
2. The diagonal of the dynamical self-energy on the Matsubara axis is then analytically continued to the real frequency axis.

3. Using the density ρ_0 from the initial mean-field calculation, construct the effective Fock exchange potential V_x .
4. Solve the quasiparticle equation for the i th spin-orbital:

$$\epsilon_i^{GW} - \epsilon_i^0 = \langle \psi_i | [\Sigma_{ii}(\epsilon_i^{GW} - \mu) + V_x - V_{xc}] | \psi_i \rangle, \quad (11)$$

where ϵ_i^0 are the eigenvalues of the underlying mean-field reference, and V_{xc} is the exchange-correlation potential, and μ is the chemical potential for G_0 .

In addition to quasiparticle energies, the spectral function is another quantity of interest and provides information about the satellites and peak widths. The G_0W_0 spectral function is defined as

$$A_{G_0W_0}(\omega) = -\frac{1}{\pi} \text{Im} \text{Tr} \mathbf{G}_{G_0W_0}(\omega), \quad (12a)$$

$$\mathbf{G}_{G_0W_0}^{-1}(\omega) = (\omega + \mu) \mathbf{S} - \mathbf{F}^{(0)} - \mathbf{V}_x - \text{diag} \Sigma(\omega) + \mathbf{V}_{xc}. \quad (12b)$$

For G_0W_0 spectral functions studied here, we observe no noticeable difference between analytical continuation of the full Green's function, and reconstruction of $G(\omega)$ from the diagonal of self-energy, as in Eq. (12b). For initializing all the calculations, we use a DFT mean-field reference with the PBE functional for solids, and a HF reference for molecules.

B. Quasiparticle self-consistent GW-I

The quasiparticle self-consistent GW (qpGW-I) method, proposed by van Schilfgaarde et al. [70, 71], aims to address the issue of reference dependence in G_0W_0 , while maintaining accuracy in band gap predictions. In qpGW-I, an effective static exchange-correlation potential $V_{\text{qsGW}}^{\text{eff}}$ is constructed from the dynamical self-energy at each iteration. Using this effective potential, a quasiparticle equation, similar to Eq. (11), is solved. In the original work in Ref. 70, two different versions of qpGW-I were proposed, labelled as scheme A and B. Here, we limit our discussion to the latter, which is easier to implement within the imaginary-time framework. The algorithm used in this work closely follows the one employed in Ref. 14. We initialize our calculation with the mean-field quasiparticle eigenvalues $\epsilon_i^{(0)}$ and eigenvectors $\mathbf{C}^{(0)}$, along with the corresponding Green's function $\mathbf{G}^{(0)}$ and density matrix $\rho^{(0)}$ and adopt the following algorithm:

1. At the n th iteration, construct the dynamical self-energy $\Sigma^{(n)}(i\omega)$ on the Matsubara axis using Eq. (6). This self-energy is then transformed from the AO basis to the quasiparticle basis as,

$$\Sigma_{\text{qp}}^{(n)}(i\omega) = \mathbf{C}^{(n-1)\dagger} \Sigma^{(n)}(i\omega) \mathbf{C}^{(n-1)}. \quad (13)$$

- The diagonal of $\Sigma_{\text{qp}}^{(n)}(i\omega)$ is analytically continued to the real frequency axis using Padé or Nevanlinna method.
- We then construct the effective exchange-correlation potential using the description:

$$\left[V_{\text{qsGW}}^{\text{eff},(n)} \right]_{ii} = \left[\Sigma_{\text{qp}}^{(n)} \right]_{ii} \left(\omega = \epsilon_i^{(n-1)} \right), \quad (14a)$$

$$\left[V_{\text{qsGW}}^{\text{eff},(n)} \right]_{ij} = \left[\Sigma_{\text{qp}}^{(n)} \right]_{ij} \left(\omega = 0 \right) \quad \forall i \neq j. \quad (14b)$$

For the diagonal entries, we utilize analytically continued self-energy, whereas in off-diagonal terms arising from $\omega = 0$, we leverage the fact that $\Sigma(\omega = 0) = \Sigma(i\omega = 0)$. Therefore, the zero-frequency contribution is obtained by interpolating the Matsubara self-energy using a four-point quadrature. This avoids any potential noise that may be introduced in AC.

- Similarly, using the density matrix $\rho^{(n-1)}$ from previous iteration, we construct the static self-energy $\Sigma_{\infty}^{(n)}$, which contains the Hartree and static exchange terms. With this, we define the new Fock operator as:

$$\mathbf{F}^{(n)} = \mathbf{H}_0 + \Sigma_{\infty}^{(n)} + \mathbf{V}_{\text{qsGW}}^{\text{eff},(n)}. \quad (15)$$

- The eigenvalues $\epsilon^{(n)}$ of the effective Fock matrix $\mathbf{F}^{(n)}$ represent the updated quasiparticle energies, while the eigenvectors $\mathbf{C}^{(n)}$ can be used to construct the new density matrix and Green's function as:

$$\rho_{\mu\nu}^{(n)} = \sum_{i \in \text{occ}} C_{\mu i}^{(n)} C_{\nu i}^{*(n)}, \quad (16a)$$

$$\mathbf{G}^{(n)}(i\omega) = \left[(i\omega + \mu)\mathbf{S} - \mathbf{F}^{(n)} \right]^{-1}, \quad (16b)$$

where the chemical potential μ is adjusted to enforce the correct number of electrons. Note that in this algorithm, the diagonalization of Fock matrix is performed only once per qpGW-I iteration. Alternatively, as suggested in the original formulation of qpGW-I, the quasiparticle equation can be solved iteratively to achieve self-consistency between $F^{(n)}$ and $\rho^{(n)}$. However, the absence of this inner self-consistency has been shown not to bear no impact on the final results. [13, 14]

- These steps are repeated until convergence is reached, for which, one may look at the difference in the density matrix,

$$\Delta\rho = \frac{1}{N_k} \frac{1}{2N_{\text{AO}}} \left| \rho^{(n)} - \rho^{(n-1)} \right|. \quad (17)$$

In practice, however, we find it easier to enforce convergence based on a combination of total energy

and band gap (IP) for solids (molecules). To enable a better convergence, we also damp the effective qpGW-I potential such that at the n th iteration, we have

$$V_{\text{qsGW}}^{\text{eff}} = \alpha V_{\text{qsGW}}^{\text{eff},(n)} + (1 - \alpha) V_{\text{qsGW}}^{\text{eff},(n-1)}, \quad (18)$$

where $\alpha = 0.7$ suffices in most cases.

The converged quasiparticle energies can be used to calculate the band gap, IP, and density of states (or spectral function). We would like to note that while tight convergence thresholds are desirable, in practice, for solids we consider a qpGW-I calculation converged if the difference in successive band gaps is less than 0.01 eV and that in total energy is less than 1 mE_h . For molecules, the problems are less severe and converging IPs to within 1 meV is generally possible.

C. Quasiparticle self-consistent GW-II

The qpGW-II approximation, also referred as the QP-2 self-consistency scheme in the literature, reduces the dynamical self-energy to an effective static term by a first-order Taylor-series expansion. Since the scheme was originally proposed in the Matsubara formalism, our implementation avoids the additional dependence on analytic continuation. Like all other methods, qpGW-II is also initialized with mean-field Fock and density matrices, $\mathbf{F}^{(0)}$ and $\rho^{(0)}$. The iterations of qpGW-II can be described as:

- Construct the static and dynamical parts of the self-energy $\Sigma_c^{(n)}$ for n th iteration, and update the Fock matrix as

$$\mathbf{F}^{(n)} = \mathbf{H}_0 + \Sigma_{\infty}^{(n)}. \quad (19)$$

This step is similar to the first step of scGW algorithm.

- Diagonalize $\mathbf{F}^{(n)}$ to obtain molecular orbitals $\mathbf{C}^{(n)}$ and eigenvalues $\epsilon^{(n)}$.
- The first non-trivial step in qpGW-II is the linear-order Taylor expansion of the Matsubara self-energy:

$$\Sigma(i\omega) \simeq \Sigma_0 + \left. \frac{\partial \Sigma(i\omega)}{\partial (i\omega)} \right|_{\omega=0} (i\omega), \quad (20)$$

where $\Sigma_0 = \Sigma(i\omega = 0)$. Substituting this approximation in Eq. (8), we get

$$\mathbf{G}^{-1}(i\omega) = i\omega \mathbf{Z}^{-1} + \mu \mathbf{S} - \mathbf{F} - \Sigma_0, \quad (21)$$

where the quasiparticle renormalization (or mass) term \mathbf{Z}^{-1} is defined as

$$\mathbf{Z}^{-1} = \mathbf{S} - \left. \frac{\partial \Sigma}{\partial (i\omega)} \right|_{\omega=0}. \quad (22)$$

4. In the orthonormal basis composed of molecular orbitals $\mathbf{C}^{(n)}$ (obtained in step 2), the Dyson equation reads as

$$\mathbf{G}_{\text{MO}}^{-1}(i\omega) = i\omega\mathbf{Z}_{\text{MO}}^{-1} + \mu - \epsilon - \Sigma_{0,\text{MO}}. \quad (23)$$

The transformation of every quantity \mathbf{X} in Eq. (21) to \mathbf{X}_{MO} in Eq. (23) is defined as

$$\mathbf{X}_{\text{MO}} = \mathbf{C}^{(n)\dagger}\mathbf{X}\mathbf{C}^{(n)}. \quad (24)$$

Readjusting the terms in Eq. (23), we obtain:

$$\mathbf{Z}_{\text{MO}}^{1/2}\mathbf{G}_{\text{MO}}^{-1}\mathbf{Z}_{\text{MO}}^{1/2} = i\omega - \mathbf{H}_{\text{eff,MO}}, \quad (25)$$

where the effective Hamiltonian is defined as:

$$\mathbf{H}_{\text{eff,MO}} = \mathbf{Z}_{\text{MO}}^{1/2}[\epsilon - \mu + \Sigma_{0,\text{MO}}]\mathbf{Z}_{\text{MO}}^{1/2}. \quad (26)$$

5. The second, and perhaps more serious, approximation invoked in qpGW-II is $\mathbf{Z}_{\text{MO}}^{-1} \approx \mathbb{I}$, where \mathbb{I} is the identity matrix. Consequently, we drop the quasiparticle mass from the left hand side of Eq. (25). However, the dependence of the effective Hamiltonian on $\mathbf{Z}_{\text{MO}}^{-1}$ in Eq. (26) is retained. Finally, we obtain a new Green's function with an approximated Dyson equation as

$$\left[\mathbf{G}^{(n+1)}\right]^{-1}(i\omega) = i\omega\mathbf{S} - \mathbf{H}_{\text{eff}}^{(n)}, \quad (27)$$

with the AO-basis effective Hamiltonian defined as

$$\mathbf{H}_{\text{eff}}^{(n)} = \mathbf{S}\zeta^{(n)}\left(\mathbf{F}^{(n)} - \mu\mathbf{S} + \Sigma_0^{(n)}\right)\zeta^{(n)\dagger}\mathbf{S}. \quad (28)$$

Here, we have as an intermediate

$$\zeta^{(n)} = \mathbf{C}^{(n)}\left[\mathbf{Z}_{\text{MO}}^{(n)}\right]^{1/2}\mathbf{C}^{(n)\dagger}. \quad (29)$$

6. Once again, the chemical potential μ is determined to maintain the correct number of electrons, and the algorithm is repeated until numerical self-consistency is achieved in the total energy. Furthermore, due to the absence of the dynamical self-energy, the Galitski-Migdal contribution E_2 vanishes in Eq. (10).

The outcome of a converged qpGW-II calculation is the effective Hamiltonian whose eigenvalue correspond to the quasiparticle energies. As a result, no analytical continuation is required in this approach. Finally, we note that convergence thresholds similar to those in scGW are enforced for qpGW-II as well.

III. COMPUTATIONAL DETAILS

The primary goal of our work is to compare different versions of the GW method, while keeping

implementation details fairly uniform. To ensure that, we employ Gaussian orbitals (or their periodic extension) as a single-particle basis of atomic orbitals. In particular, for solids, we use the GTH-DZVP-MOLOPT-SR basis-sets, with the corresponding GTH-PBE pseudopotentials. For molecular test-set, we perform all-electron calculations using the cc-pVQZ basis-sets. Basis-set extrapolation is not performed for either set of systems. For two-electron integrals, we use the density-fitting approximation [88] implemented in PySCF package (version 2.0.1) [89, 90]. Specifically, we use the def2-tzvp-jkfit and cc-pVQZ-jkfit basis-sets as the auxiliary basis-set for density-fitting in solids and molecules, respectively. We note that in GTH pseudopotentials for Zn and Ga, the valence shell 3d orbital is considered as a part of the core. As a result, the correlation effects arising from these orbitals are not well recovered.

Dynamical quantities that depend on the imaginary time and frequency are represented using highly accurate yet compact intermediate-representation (IR) grids [91, 92]. All the GW calculations are performed at an inverse temperature $\beta = 1000 \text{ a.u.}^{-1}$. For the analytical continuation of Matsubara Green's function and self-energy diagonal, we use both Nevanlinna [79] and Padé [77] methods, often interchangeably, and find that they provide almost identical results for quasiparticle peaks. Using the Padé approach also allows us to establish equivalence with previous implementations. In order to avoid poles on the real axis, when performing analytical continuation, we keep a small imaginary component η for the frequency, i.e.,

$$X(i\omega_n) \xrightarrow[\text{Continuation}]{\text{Analytical}} X(\omega + i\eta). \quad (30)$$

This leads to a broadening of the spectral features which is inherently different from the broadening induced by the imaginary part of self-energy. For obtaining band gaps from scGW, we employ $\eta = 0.001 \text{ a.u.}$, which provides sharp and well-resolved quasiparticle peaks. For the AC step in qpGW-I, for most systems, we use $\eta = 0.01 \text{ a.u.}$

Other than Ewald summation for the Fock exchange [93–95], no finite-size corrections have been used for any of the GW or DFT results. Instead, band gaps have been extrapolated from calculations with $4 \times 4 \times 4$ and $6 \times 6 \times 6$ k -point samplings in the Brillouin zone (BZ), assuming a linear relation between the band gap and the inverse cube root of the number of k -points in the BZ. For carbon and silicon, calculations with $6 \times 6 \times 6$ and $8 \times 8 \times 8$ k -points were used for extrapolation. We also note that all DFT band gaps were calculated using a $6 \times 6 \times 6$ k -points sampling.

Before we proceed to the Results section, it is worthwhile to comment on the need for accurate grids for dynamical quantities, especially in a scGW calculation. In a typical cycle of GW, one needs to transform G , Σ and Π , between the imaginary time and Matsubara frequency axes (cf. Section II A 1). Furthermore, adjusting the chemical potential triggers a fair amount of

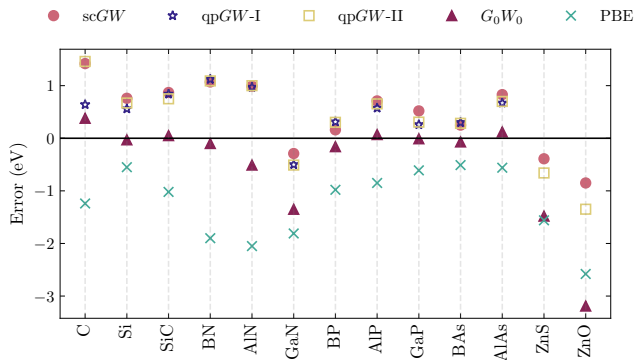


FIG. 2. Band gap errors, with respect to experiment, for selected semiconductors and insulators, as predicted by full and quasiparticle self-consistent GW methods. PBE and G_0W_0 -PBE results are also included for reference.

$G(i\omega) \leftrightarrow G(\tau)$ operations. The Green's function would quickly accumulate detrimental amount of noise if the underlying grids do not guarantee a high accuracy in Fourier transforms. In this work, most of the calculations employ 104 IR grid points, which ensures an accuracy of 10^{-10} or better in Fourier transformations. This helps us enforce tight thresholds for total energy and particle number in $scGW$, necessary for reliable applications to real systems. Older generation of GW codes usually employ a uniform Matsubara grid, which requires several hundreds or up to a thousand grid points to ensure high accuracy. An example is the ComDMFT [96] code used in Kutepov's comparative study [83]. Similarly, for Grumet's results in Ref. 22, the early generation of sparse grids [97] appears to afford merely 5-6 iterations of $scGW$ and a particle number fluctuation of $\sim 10^{-3}$. Development of accurate imaginary time and Matsubara grids has been an active area of research [91, 97–101], culminating in the developments of accurate grids such as IR [91] and discrete Lehmann representation [100] grids.

IV. RESULTS

Electronic structure methods are best compared when multiple properties in different kinds of systems are analyzed. For a thorough analysis of the GW methods, we compare band gaps in insulating solids, as well as IPs in molecules. Additionally, we take a closer look at the spectral function from different methods, while also scrutinizing their convergence trends.

A. Band gaps in insulators

First, we analyze the band gaps in selected insulators and semiconductors. This is captured in Fig. 2 where we compare $scGW$, $qpGW$ -I, and $qpGW$ -II. We also show results for PBE and G_0W_0 -PBE. The corresponding

numerical data, along with existing reference values from the literature, are also presented in Table I, along with the crystal structures and lattice constants. Our results unequivocally show that for band gaps, quasiparticle and fully self-consistent GW methods produce very similar results. On the other hand, consistent with existing literature, we find that while PBE generally underestimates the band gaps, G_0W_0 -PBE appears to be the most accurate among all the methods. It is sometimes presumed that $scGW$ severely over-estimates band gaps, while $qpGW$ improves upon it. However, the results in Table I do not support such claims.

For ZnS, ZnO and GaN, the behavior is somewhat different, i.e., G_0W_0 does not improve upon PBE, and $scGW$ appears to perform the best. In systems with Zn and Ga, the closed-shell $3d$ orbitals, which play an important role in electron correlation, are not present in the GTH -DZVP-MOLOPT-SR basis-set, and instead treated as part of the pseudopotential core.

It is worth mentioning that converging the GW calculations with respect to basis-set size, in an all-electron setting, generally leads to more accurate band gaps. For instance, when comparing $scGW$ band gaps in this work against those in Ref. 66, it is evident that going from GTH basis-set and pseudopotential to a sufficiently large all-electron basis-set $x2c$ -TZVPA11 improves the band gaps by ~ 0.3 eV. Nevertheless, we do not expect any significant variation in the relative accuracy between different self-consistent GW methods. This is because the GTH basis-sets and pseudopotentials are well optimized (for DFT) with respect to converged plane wave calculations [106, 107]. One can expect reasonable behavior for correlated methods as well, particularly since the materials here involve light elements with negligible relativistic effects [108]. The overall quality of the different self-consistent GW results can be expected to get better with larger all-electron basis-sets.

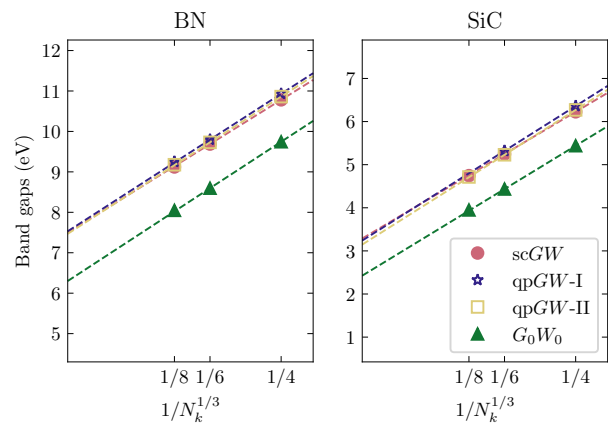


FIG. 3. Variation in BN and SiC band gaps with respect to Brillouin-zone sampling. The linear fit is performed using $N_k^{1/3} = 4$ and 6 grids. The results from $N_k^{1/3} = 8$ show excellent agreement with this fit, demonstrating the reliability of the extrapolation procedure.

TABLE I. Band gaps (in eV) for selected semiconductors and insulators, comparing PBE, G_0W_0 -PBE, quasiparticle and fully self-consistent GW methods against experimental data. Previously reported values for $scGW$, $qpGW$ -I, and $qpGW$ -II are also included for reference. For ZnO and ZnS, the $qpGW$ -I calculation could not be converged. We have used diamond lattice structure for C and Si, and zinblende for all other systems. Lattice constants a are also reported here. Experimental values for band gaps have been adopted from Refs. 22, 102–105.

Material	PBE	G_0W_0	$scGW$	$qpGW$ -I	$qpGW$ -II	Exp.	Other $scGW$		Other $qpGW$ -I/II				a (Å)
							Ref. 22	Ref. 83	Ref. 22	Ref. 83	Ref. 71	Ref. 85	
C	4.24	5.86	6.90	6.12	6.94	5.48	6.41	6.15	6.43	6.18	5.97	6.14	3.56
Si	0.62	1.14	1.93	1.73	1.84	1.17	2.18	1.55	1.49	1.41	1.28	1.32	5.43
SiC	1.38	2.45	3.27	3.24	3.15	2.40	3.29	2.89	2.88	2.79	2.58	2.81	4.35
BN	4.50	6.30	7.47	7.52	7.49	6.40	7.67	7.06	7.50	7.06		7.07	3.61
AlN	3.29	4.83	6.33	6.31	6.34	5.34							4.37
GaN	1.59	2.05	3.11	2.90	2.89	3.40	3.94		3.78				4.53
BP	1.42	2.24	2.56	2.71	2.70	2.40							4.53
AlP	1.60	2.52	3.16	3.03	3.10	2.45	3.20	2.84	2.94	2.80		2.76	5.46
GaP	1.65	2.25	2.78	2.52	2.57	2.26	2.77		2.67				5.45
BAs	1.31	1.75	2.07	2.12	2.10	1.82							4.77
AlAs	1.60	2.28	2.99	2.83	2.86	2.16	2.98		2.84				5.66
ZnS	2.04	2.12	3.21		2.94	3.60	4.68	4.28	4.27	4.19	4.13		5.42
ZnO	0.66	0.05	2.39		1.89	3.24	4.92		4.29				4.58

1. Finite-size extrapolation

The band gaps presented here are calculated using linear extrapolation of results from $N_k^{1/3} = 4, 6$ as mentioned in Section III. To validate that these two grid-samplings are sufficient to extrapolate from, for SiC and BN as examples, we have also performed calculations using an $8 \times 8 \times 8$ k -mesh. The resultant $N_k^{1/3} = 8$ band gaps show excellent agreement with the linear fits derived from $N_k^{1/3} = 4$ and $N_k^{1/3} = 6$ data. This result is summarized in Fig. 3. The use of linear extrapolation technique ensures that finite-size corrections and associated approximations do not influence the comparison between different methods.

2. Convergence trends

In Fig. 4, we study the trends in band gaps and total energy per unit cell for SiC, BN and ZnS as we iterate through different self-consistency schemes. First, we observe that for all three materials, it is fairly straightforward to impose tight convergence criterion in $scGW$ and $qpGW$ -II. Even without the use of convergence acceleration techniques such as direct inversion of iterative subspace [109], both these methods converge the total energy to within 10^{-5} a.u., and band gaps to within 10^{-4} eV in 10-20 iterations. Contrarily, extra care is required in $qpGW$ -I, where we rely on trends

in both band gap (or IPs) and total energy to establish convergence. For solids, tight convergence was achievable only for small systems like SiC and BN, and for the general case, the band gaps are converged only at the level of 0.01 eV. For ZnS and ZnO (not shown here), we could not converge $qpGW$ -I. This is likely due to the complexity of electron correlation brought by the transition metal. Similar challenges have been noted in the literature [85].

3. Spectral functions

One of the concerns surrounding $scGW$ is its inability to describe plasmon satellites, which are, however, captured by G_0W_0 . This behavior was first noted by Holm et al. for the electron gas [61], where iterations of self-consistency were observed to completely diminish sharp satellites. Similar trends have been reported for diamond by Grumet et al. [22]. In Fig. 5, we compare G_0W_0 -PBE, $scGW$ and $qpGW$ -II spectral functions for diamond for the Γ_1 and Γ_{25} bands, with the first two computed using the Padé continuation. Strikingly, we find that $scGW$ is able to capture the plasmon satellites for both the bands. However, the weight of the satellites is smaller than G_0W_0 , supporting existing knowledge that self-consistency leads to an increased quasiparticle weight. Comparing with similar results in existing literature, we note that our $scGW$ is capable of predicting satellite features where earlier works could

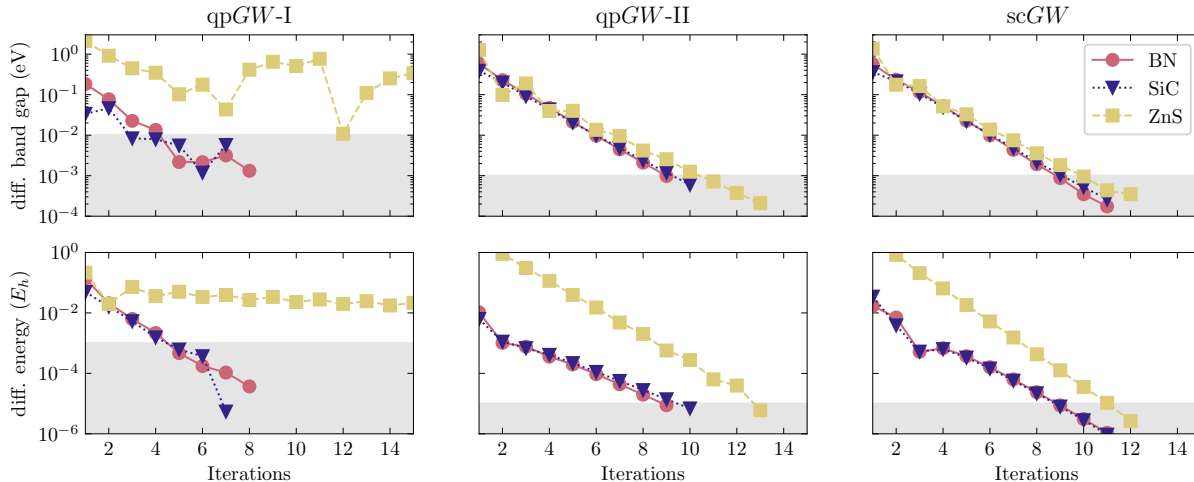


FIG. 4. Convergence trends for band gaps (eV) and total energy per unit cell (E_h) for qpGW-I, qpGW-II and scGW, all calculated for $4 \times 4 \times 4$ k -mesh sampling in the BZ. We consider SiC and BN as typical examples of easy convergence, while ZnS proves to be a challenging system for qpGW-I.

not. We speculate that this improvement is a result of superior quality of time and frequency grids, as well as strong convergence criteria on both particle number and total energies. These results should be contrasted with quasiparticle self-consistent GW schemes, which, by definition, do not retain any information about satellite structures in the spectral function.

B. Ionization potentials in molecules

Comparison of different self-consistency schemes such as scGW and qpGW-I have been relatively scarce in the context of molecular systems as well [11, 62]. Moreover,

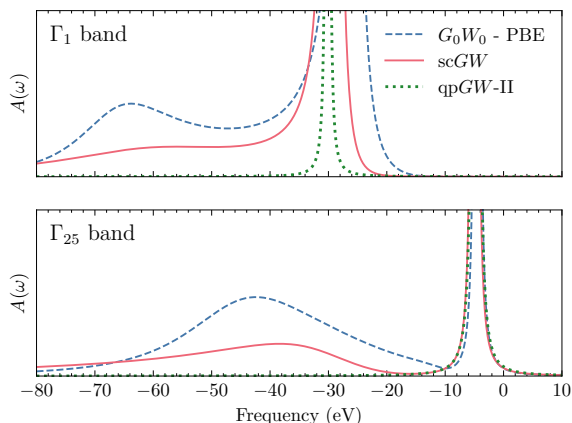


FIG. 5. Spectral function for the Γ_1 and Γ_{25} bands in diamond, calculated using G_0W_0 -PBE, scGW and qpGW-II. The results use a $6 \times 6 \times 6$ k -mesh, and Padé analytical continuation for G_0W_0 and scGW. The y -axis is magnified to emphasize the satellites.

to our knowledge, application of the qpGW-II scheme to molecules has not been explored in the literature. Here, we bridge this gap with our implementation and benchmark various GW self-consistency schemes for predicting IPs across a selection of 29 molecules. This molecular dataset was originally used by Maggio et al. [12] to benchmark vertex corrections on G_0W_0 methods. Recently, Wen et al. [15] also used this dataset to show that scGW, with the same implementation as is used in this work, provides accurate IPs, comparable in quality with vertex-corrected G_0W_0 methods.

In Table II, we compare the mean absolute error (MAE) and standard deviation of error (SD) with respect to both the experiment and $\Delta\text{CCSD(T)}$, for the prediction of IP in these molecules. Complete set of IP values are presented in Table III of Appendix A. The G_0W_0 -HF, scGW, and the $\Delta\text{CCSD(T)}$ results are taken from Ref. 15, while calculations for the quasiparticle self-consistent methods are carried out with the implementations discussed in Section II. Unlike in solids, where full and quasiparticle self-consistency results in similar band gaps, for molecular IPs, scGW clearly outperforms qpGW-I and qpGW-II. With respect to experiment, the MAE of 0.30 eV in scGW is much smaller than 0.42 eV and 0.44 eV in qpGW-I and qpGW-II, respectively. The standard deviations in all the methods, including G_0W_0 -HF, are similar in magnitude. It is interesting to note that with respect to $\Delta\text{CCSD(T)}$, the quasiparticle and fully self-consistent GW methods exhibit comparable MAE and SD. We also note that the qpGW-I and qpGW-II results are very close to each other for molecular IPs. As mentioned in Section III, all the results have been calculated using the cc-pVQZ basis. Considering the large size of this basis, we anticipate that extrapolation to complete basis-set limit will not introduce any significant change in overall trends.

TABLE II. Mean absolute error (MAE) and associated standard deviation (SD) in eV for different self-consistent GW methods for the 29-molecule data-set. $\Delta\text{CCSD(T)}$ results are also included for reference. ^aResults adopted from Ref. 15.

Method	w.r.t experiment		w.r.t. $\Delta\text{CCSD(T)}$	
	MAE	SD	MAE	SD
$G_0W_0\text{-HF}^a$	0.65	0.36	0.49	0.28
$\text{sc}GW^a$	0.30	0.27	0.24	0.20
$\text{qp}GW\text{-I}$	0.42	0.32	0.28	0.14
$\text{qp}GW\text{-II}$	0.44	0.31	0.29	0.16
$\Delta\text{CCSD(T)}^a$	0.23	0.32	-	-

In terms of convergence, $\text{qp}GW\text{-I}$ in molecules exhibits a much better behavior, and in most cases, IPs can be systematically converged to less than 10^{-3} eV in 10-20 iterations. With the exception of CO, SiO, and CS, all other IPs are well converged. For $\text{sc}GW$ and $\text{qp}GW\text{-II}$, we do not encounter any convergence issues.

V. CONCLUSION

We have presented a comprehensive analysis of quasiparticle self-consistent GW methods against their one-shot and fully self-consistent counterparts. We have employed finite-temperature Green’s functions and maintained identical technical details for all the methods, ensuring a fair comparison free of inconsistencies arising from differences in implementations. Our aim is to compare different self-consistent schemes available in the GW community and our observations are based on analysis of three key measures, namely (i) band gap recovery for solids and IP recovery for molecules, (ii) convergence characteristics of each of the schemes, and (iii) recovery of spectral features.

The band gap recovery, for simple semiconductors considered in a Gaussian basis, was very similar for all the self-consistency schemes. These observations reinforce findings in Refs. 22 and 83 who also observed that the band gaps from $\text{qp}GW\text{-I}$ and $\text{qp}GW\text{-II}$ schemes are very close to $\text{sc}GW$ values. When molecules are considered, we found that $\text{sc}GW$ was clearly superior to $\text{qp}GW\text{-I}$ and $\text{qp}GW\text{-II}$ for the recovery of the IPs. Furthermore, both the $\text{qp}GW$ methods produced results of similar quality.

We have observed that while all the values of the band gaps remained relatively agnostic to the self-consistency scheme, the convergence characteristics did not. For solids, we experienced much more difficulties converging the $\text{qp}GW\text{-I}$ scheme than $\text{sc}GW$ and $\text{qp}GW\text{-II}$. Moreover, we were unable to converge $\text{qp}GW\text{-I}$ to the same accuracy as the two other schemes. For molecules, we observed fewer convergence difficulties in the $\text{qp}GW\text{-I}$ scheme and it was generally possible to converge IPs to less than 10^{-3} eV.

The primary quasiparticle peaks are well recovered in all the self-consistency schemes. Both $\text{qp}GW\text{-I}$ and $\text{qp}GW\text{-II}$ are by definition incapable of illustrating any other features than these primary peaks in the spectrum. Remarkably, the plasmon satellites are preserved by $\text{sc}GW$ in the diamond lattice carbon studied here, although their weight is reduced in comparison with G_0W_0 results. Comparing with earlier works, such as Ref. 22, we speculate that this improvement in our version of $\text{sc}GW$ is a result of superior quality of time and frequency grids, as well as strong convergence criteria on both particle number and total energies which were not present in the earlier works. It should be noted however that despite this success of $\text{sc}GW$ in the recovery of the plasmon satellites, we can still expect that accurate illustration of some of the spectral features will require higher-level Feynman diagrams than the ones present in the GW self-energy.

Furthermore, the evaluation of total energy makes sense only for $\text{sc}GW$, where thermodynamic properties are uniquely defined. The absence of reliable total energy may not be a concern in solids since the cohesive energy of a unit cell is rarely of interest. In contrast, the ability to calculate energies is of paramount importance in molecules since most calculations rely on the evaluation of energy differences. However, even when the calculation of total energy or energy differences may be avoided, other observable quantities, even as simple as orbital occupation or more complicated correlation functions are also uniquely defined only for $\text{sc}GW$.

Considering all these observations and knowing that the development of highly accurate, yet compact, grids together with additional integral factorization schemes make the $\text{sc}GW$ scheme already quite computationally accessible, one can arrive at following practical recommendations on when the different schemes should be used. Only in lighter accuracy calculations when the tight convergence of the IP or band gap values is not necessary, and only primary quasiparticle peaks are of interest, and additionally only very limited in memory is available, $\text{qp}GW\text{-I}$ or $\text{qp}GW\text{-II}$ may be beneficial since in this method at the start of each iteration, the Green’s function is reset to a mean-field object, thus partially alleviating some of the memory bottlenecks. In all the other cases, $\text{sc}GW$ method will be superior due to smoother convergence, good band gap recovery, possibility of observing more spectral features, and well defined evaluation of thermodynamic quantities including energy.

ACKNOWLEDGMENTS

This material is based upon work supported by the U.S. Department of Energy, Office of Science, Office of Advanced Scientific Computing Research and Office of Basic Energy Sciences, Scientific Discovery through Advanced Computing (SciDAC) program under Award

Number DE-SC0022198. This research used resources of the National Energy Research Scientific Computing Center, a DOE Office of Science User Facility supported by the Office of Science of the U.S. Department of Energy under Contract No. DE-AC02-05CH11231 using NERSC award BES-ERCAP0029462 and BES-ERCAP0024293. We also acknowledge helpful discussion with Dr. Chian-Nan Yeh and Dr. Arno Förster.

Appendix A: Ionization potential data for molecules

Detailed ionization potential data for the 29 molecules studied in Table II is presented here in Table III. For

N_2 , ClF and HClO, the qpGW-I loop (marked with a * in Table III) was terminated once the IP was converged to within 0.001 eV. For CO, SiO and CS, we could not converge the qpGW-I results (marked with ** in Table III) even after 20 iterations. For all these calculations, we have employed the cc-pVQZ basis-set. Furthermore, all calculated IPs assume vertical ionization, i.e., the geometry of the ionized molecule is not relaxed. Among experimental results, the vertical IP values are shown in italics. The discrepancy between experiment and theory is generally larger when the IPs that are non-vertical in nature. For such systems, comparing the GW methods against Δ CCSD(T), while assuming vertical ionization, may be more sensible.

-
- [1] L. Hedin, New Method for Calculating the One-Particle Green's Function with Application to the Electron-Gas Problem, *Phys. Rev.* **139**, A796 (1965).
- [2] F. Aryasetiawan and O. Gunnarsson, The GW method, *Rep. Prog. Phys.* **61**, 237 (1998).
- [3] L. Reining, The GW approximation: content, successes and limitations, *WIREs Comp. Mol. Sci.* **8**, e1344 (2018).
- [4] D. Golze, M. Dvorak, and P. Rinke, The GW Compendium: A Practical Guide to Theoretical Photoemission Spectroscopy, *Front. Chem.* **7**, 10.3389/fchem.2019.00377 (2019).
- [5] W. Kohn and J. M. Luttinger, Ground-State Energy of a Many-Fermion System, *Phys. Rev.* **118**, 41 (1960).
- [6] W. Kohn and L. J. Sham, Self-Consistent Equations Including Exchange and Correlation Effects, *Phys. Rev.* **140**, A1133 (1965).
- [7] A. Stan, N. E. Dahlen, and R. v. Leeuwen, Fully self-consistent GW calculations for atoms and molecules, *EPL* **76**, 298 (2006).
- [8] F. Caruso, P. Rinke, X. Ren, M. Scheffler, and A. Rubio, Unified description of ground and excited states of finite systems: The self-consistent GW approach, *Phys. Rev. B* **86**, 081102 (2012).
- [9] N. Marom, F. Caruso, X. Ren, O. T. Hofmann, T. Körzdörfer, J. R. Chelikowsky, A. Rubio, M. Scheffler, and P. Rinke, Benchmark of GW methods for azabenzenes, *Phys. Rev. B* **86**, 245127 (2012).
- [10] M. J. van Setten, F. Weigend, and F. Evers, The GW-Method for Quantum Chemistry Applications: Theory and Implementation, *J. Chem. Theory Comput.* **9**, 232 (2013).
- [11] F. Caruso, M. Dauth, M. J. van Setten, and P. Rinke, Benchmark of GW Approaches for the GW100 Test Set, *J. Chem. Theory Comput.* **12**, 5076 (2016).
- [12] E. Maggio and G. Kresse, GW Vertex Corrected Calculations for Molecular Systems, *J. Chem. Theory Comput.* **13**, 4765 (2017).
- [13] A. Förster and L. Visscher, Low-Order Scaling G0W0 by Pair Atomic Density Fitting, *J. Chem. Theory Comput.* **16**, 7381 (2020).
- [14] A. Förster and L. Visscher, Low-Order Scaling Quasiparticle Self-Consistent GW for Molecules, *Front. Chem.* **9** (2021).
- [15] M. Wen, V. Abraham, G. Harsha, A. Shee, K. B. Whaley, and D. Zgid, Comparing self-consistent gw and vertex-corrected g0w0 (G0W0 Γ) accuracy for molecular ionization potentials, *J. Chem. Theory Comput.* **20**, 3109 (2024).
- [16] V. Abraham, G. Harsha, and D. Zgid, Relativistic Fully Self-Consistent GW for Molecules: Total Energies and Ionization Potentials, *J. Chem. Theory Comput.* **20**, 4579 (2024).
- [17] S. V. Faleev, M. van Schilfgaarde, and T. Kotani, All-Electron Self-Consistent GW Approximation: Application to Si, MnO, and NiO, *Phys. Rev. Lett.* **93**, 126406 (2004).
- [18] M. Shishkin and G. Kresse, Self-consistent GW calculations for semiconductors and insulators, *Phys. Rev. B* **75**, 235102 (2007).
- [19] A. Kutepov, S. Y. Savrasov, and G. Kotliar, Ground-state properties of simple elements from GW calculations, *Phys. Rev. B* **80**, 041103 (2009).
- [20] F. Bruneval and M. Gatti, Quasiparticle Self-Consistent GW Method for the Spectral Properties of Complex Materials, in *First Principles Approaches to Spectroscopic Properties of Complex Materials*, Topics in Current Chemistry, edited by C. Di Valentin, S. Botti, and M. Cococcioni (Springer, Berlin, Heidelberg, 2014) pp. 99–135.
- [21] A. L. Kutepov, Ground state properties of 3d metals from self-consistent GW approach, *J. Phys.: Condens. Matter* **29**, 465503 (2017).
- [22] M. Grumet, P. Liu, M. Kaltak, J. Klimeš, and G. Kresse, Beyond the quasiparticle approximation: Fully self-consistent GW calculations, *Phys. Rev. B* **98**, 155143 (2018).
- [23] P. Pokhilko and D. Zgid, Broken-symmetry self-consistent GW approach: Degree of spin contamination and evaluation of effective exchange couplings in solid antiferromagnets, *J. Chem. Phys.* **157**, 144101 (2022).
- [24] P. Pokhilko and D. Zgid, Evaluation of Neel Temperatures from Fully Self-Consistent Broken-Symmetry GW and High-Temperature Expansion: Application to Cubic Transition-Metal Oxides, *J. Phys. Chem. Lett.* **14**, 5777 (2023).

TABLE III. The first ionization potential (eV) data for 29 molecules. All the calculations were performed using cc-pVQZ basis-set. Italicized values are for the vertical IPs. *Only converged in IP values, not total energies. **Not converged.

Molecule	$\Delta\text{CCSD(T)}$ [12]	$G_0W_0\text{-HF}$ [15]	scGW [15]	qpGW-I	qpGW-II	Exp. [110–133]
H ₂	-16.39	-16.59	-16.24	-16.53	-16.55	-15.43
Li ₂	-5.17	-5.38	-4.94	-5.37	-5.34	-4.73
N ₂	-15.49	-16.56	-15.57	-15.98*	-16.06	-15.58
P ₂	-10.76	-10.71	-9.85	-10.60	-10.51	-10.62
Cl ₂	-11.62	-11.98	-11.24	-11.84	-11.72	<i>-11.49</i>
CH ₄	-14.40	-14.92	-14.32	-14.68	-14.76	<i>-13.6</i>
C ₂ H ₄	-10.69	-10.88	-10.18	-10.65	-10.66	<i>-10.68</i>
C ₂ H ₂	-11.42	-11.77	-10.96	-11.50	-11.54	<i>-11.49</i>
SiH ₄	-12.82	-13.35	-12.80	-13.17	-13.20	<i>-12.3</i>
LiH	-7.94	-8.28	-7.94	-8.31	-8.22	-7.9
NH ₃	-10.92	-11.40	-10.86	-11.17	-11.23	-10.82
PH ₃	-10.49	-10.92	-10.28	-10.75	-10.75	<i>-10.59</i>
H ₂ S	-10.43	-10.69	-10.09	-10.51	-10.55	<i>-10.50</i>
HF	-16.09	-16.49	-16.26	-16.52	-16.59	<i>-16.12</i>
NaCl	-9.13	-9.43	-8.93	-9.48	-9.33	<i>-9.80</i>
HCN	-13.64	-14.07	-13.22	-13.81	-13.82	<i>-13.61</i>
N ₂ H ₄	-10.24	-10.38	-9.71	-10.11	-10.16	<i>-8.98</i>
CH ₃ OH	-11.08	-11.79	-11.16	-11.53	-11.59	<i>-10.96</i>
H ₂ O ₂	-11.49	-12.32	-11.66	-12.08	-12.12	<i>-11.70</i>
H ₂ O	-12.64	-13.11	-12.73	-12.99	-13.06	<i>-12.62</i>
CO ₂	-13.78	-14.46	-13.66	-14.16	-14.16	<i>-13.77</i>
CO	-14.05	-15.25	-14.08	**	-14.57	<i>-14.01</i>
SO ₂	-12.41	-13.16	-12.21	-12.90	-12.70	<i>-12.50</i>
ClF	-12.82	-13.29	-12.49	-13.13	-13.01	<i>-12.77</i>
CH ₃ Cl	-11.41	-11.76	-11.16	-11.60*	-11.66	<i>-11.29</i>
CH ₃ SH	-9.49	-9.84	-9.16	-9.66	-9.70	<i>-9.44</i>
SiO	-11.55	-12.04	-11.25	**	-11.69	-11.3
CS	-11.45	-12.55	-11.34	**	-11.83	-11.33
HClO	-11.30	-11.84	-11.10	-11.54*	-11.59	-11.12
MAE from exp.	0.23	0.65	0.30	0.42	0.44	
MAE from $\Delta\text{CCSD(T)}$		0.49	0.24	0.28	0.29	

[25] S. Biermann, F. Aryasetiawan, and A. Georges, First-principles approach to the electronic structure of strongly correlated systems: Combining the *gw* approximation and dynamical mean-field theory, *Phys. Rev. Lett.* **90**, 086402 (2003).

[26] G. Kotliar, S. Y. Savrasov, K. Haule, V. S. Oudovenko, O. Parcollet, and C. A. Marianetti, Electronic structure calculations with dynamical mean-field theory, *Rev. Mod. Phys.* **78**, 865 (2006).

[27] S. Choi, A. Kutepov, K. Haule, M. van Schilfhaarde, and G. Kotliar, First-principles treatment of mott insulators: linearized qsgw+dmft approach, *npj Quant. Mater.* **1**, 16001 (2016).

[28] J. Lee and K. Haule, Diatomic molecule as a testbed for combining DMFT with electronic structure methods such as *GW* and DFT, *Phys. Rev. B* **95**, 155104 (2017).

[29] F. Nilsson, L. Boehnke, P. Werner, and F. Aryasetiawan, Multitier self-consistent *GW* + EDMFT, *Phys. Rev. Materials* **1**, 043803

- (2017).
- [30] T. Zhu and G. K.-L. Chan, Ab initio full cell gw +DMFT for correlated materials, *Phys. Rev. X* **11**, 021006 (2021).
- [31] T. N. Lan, A. Shee, J. Li, E. Gull, and D. Zgid, Testing self-energy embedding theory in combination with GW, *Phys. Rev. B* **96**, 155106 (2017).
- [32] S. Iskakov, C.-N. Yeh, E. Gull, and D. Zgid, Ab initio self-energy embedding for the photoemission spectra of nio and mno, *Phys. Rev. B* **102**, 085105 (2020).
- [33] C.-N. Yeh, S. Iskakov, D. Zgid, and E. Gull, Electron correlations in the cubic paramagnetic perovskite $Sr(V, Mn)_O_3$: Results from fully self-consistent self-energy embedding calculations, *Phys. Rev. B* **103**, 195149 (2021).
- [34] A. A. Rusakov, S. Iskakov, L. N. Tran, and D. Zgid, Self-energy embedding theory (seet) for periodic systems, *J. Chem. Theory Comput.* **15**, 229 (2019), pMID: 30540474.
- [35] S. Iskakov, A. A. Rusakov, D. Zgid, and E. Gull, Effect of propagator renormalization on the band gap of insulating solids, *Phys. Rev. B* **100**, 085112 (2019).
- [36] G. E. Scuseria, T. M. Henderson, and I. W. Bulik, Particle-particle and quasiparticle random phase approximations: Connections to coupled cluster theory, *J. Chem. Phys.* **139**, 104113 (2013).
- [37] M. F. Lange and T. C. Berkelbach, On the Relation between Equation-of-Motion Coupled-Cluster Theory and the GW Approximation, *J. Chem. Theory Comput.* **14**, 4224 (2018).
- [38] R. Quintero-Monsebaiz, E. Monino, A. Marie, and P.-F. Loos, Connections between many-body perturbation and coupled-cluster theories, *J. Chem. Phys.* **157**, 231102 (2022).
- [39] J. Tölle and G. Kin-Lic Chan, Exact relationships between the GW approximation and equation-of-motion coupled-cluster theories through the quasi-boson formalism, *J. Chem. Phys.* **158**, 124123 (2023).
- [40] O. Vahtras, J. Almlöf, and M. W. Feyereisen, Integral approximations for LCAO-SCF calculations, *Chem. Phys. Lett.* **213**, 514 (1993).
- [41] Q. Sun, T. C. Berkelbach, J. D. McClain, and G. K.-L. Chan, Gaussian and plane-wave mixed density fitting for periodic systems, *J. Chem. Phys.* **147**, 164119 (2017).
- [42] H.-Z. Ye and T. C. Berkelbach, Fast periodic Gaussian density fitting by range separation, *J. Chem. Phys.* **154**, 131104 (2021).
- [43] C.-N. Yeh and M. A. Morales, Low-Scaling Algorithms for GW and Constrained Random Phase Approximation Using Symmetry-Adapted Interpolative Separable Density Fitting, *J. Chem. Theory Comput.* **20**, 3184 (2024).
- [44] M. S. Hybertsen and S. G. Louie, Ab initio static dielectric matrices from the density-functional approach. I. Formulation and application to semiconductors and insulators, *Phys. Rev. B* **35**, 5585 (1987).
- [45] R. W. Godby and R. J. Needs, Metal-insulator transition in Kohn-Sham theory and quasiparticle theory, *Phys. Rev. Lett.* **62**, 1169 (1989).
- [46] A. Oshlies, R. W. Godby, and R. J. Needs, GW self-energy calculations of carrier-induced band-gap narrowing in n-type silicon, *Phys. Rev. B* **51**, 1527 (1995).
- [47] G. E. Engel and B. Farid, Generalized plasmon-pole model and plasmon band structures of crystals, *Phys. Rev. B* **47**, 15931 (1993).
- [48] P. Larson, M. Dvorak, and Z. Wu, Role of the plasmon-pole model in the GW approximation, *Phys. Rev. B* **88**, 125205 (2013).
- [49] T. Körzdörfer and N. Marom, Strategy for finding a reliable starting point for G_0W_0 demonstrated for molecules, *Phys. Rev. B* **86**, 041110 (2012).
- [50] F. Bruneval and M. A. L. Marques, Benchmarking the Starting Points of the GW Approximation for Molecules, *J. Chem. Theory Comput.* **9**, 324 (2013).
- [51] J. P. Perdew, K. Burke, and M. Ernzerhof, Generalized Gradient Approximation Made Simple, *Phys. Rev. Lett.* **77**, 3865 (1996).
- [52] G. Onida, L. Reining, and A. Rubio, Electronic excitations: density-functional versus many-body Green's-function approaches, *Rev. Mod. Phys.* **74**, 601 (2002).
- [53] P. Rinke, A. Qteish, J. Neugebauer, C. Freysoldt, and M. Scheffler, Combining GW calculations with exact-exchange density-functional theory: an analysis of valence-band photoemission for compound semiconductors, *New J. Phys.* **7**, 126 (2005).
- [54] F. Fuchs, J. Furthmüller, F. Bechstedt, M. Shishkin, and G. Kresse, Quasiparticle band structure based on a generalized Kohn-Sham scheme, *Phys. Rev. B* **76**, 115109 (2007).
- [55] W. Chen and A. Pasquarello, Accurate band gaps of extended systems via efficient vertex corrections in GW , *Phys. Rev. B* **92**, 041115 (2015).
- [56] S. E. Gant, J. B. Haber, M. R. Filip, F. Sagredo, D. Wing, G. Ohad, L. Kronik, and J. B. Neaton, Optimally tuned starting point for single-shot GW calculations of solids, *Phys. Rev. Mater.* **6**, 053802 (2022).
- [57] R. Rodrigues Pela, C. Vona, S. Lubeck, B. Alex, I. Gonzalez Oliva, and C. Draxl, Critical assessment of G_0W_0 calculations for 2D materials: the example of monolayer MoS_2 , *npj Comput. Mater.* **10**, 1 (2024).
- [58] L. Zhang, Y. Shu, C. Xing, X. Chen, S. Sun, Y. Huang, and D. G. Truhlar, Recommendation of Orbitals for G_0W_0 Calculations on Molecules and Crystals, *J. Chem. Theory Comput.* **18**, 3523 (2022).
- [59] J. Li, Y. Jin, P. Rinke, W. Yang, and D. Golze, Benchmark of GW Methods for Core-Level Binding Energies, *J. Chem. Theory Comput.* **18**, 7570 (2022).
- [60] A. Förster, E. van Lenthe, E. Spadetto, and L. Visscher, Two-Component GW Calculations: Cubic Scaling Implementation and Comparison of Vertex-Corrected and Partially Self-Consistent GW Variants, *J. Chem. Theory Comput.* **19**, 5958 (2023).
- [61] B. Holm and U. von Barth, Fully self-consistent GW self-energy of the electron gas, *Phys. Rev. B* **57**, 2108 (1998).
- [62] P. Koval, D. Foerster, and D. Sánchez-Portal, Fully self-consistent GW and quasiparticle self-consistent GW for molecules, *Phys. Rev. B* **89**, 155417 (2014).
- [63] H. Cao, Z. Yu, P. Lu, and L.-W. Wang, Fully converged plane-wave-based self-consistent GW calculations of periodic solids, *Phys. Rev. B* **95**, 035139 (2017).
- [64] X. Ren, F. Merz, H. Jiang, Y. Yao, M. Rampp, H. Lederer, V. Blum, and M. Scheffler, All-electron

- periodic G_0W_0 implementation with numerical atomic orbital basis functions: Algorithm and benchmarks, *Phys. Rev. Mater.* **5**, 013807 (2021).
- [65] C.-N. Yeh, A. Shee, Q. Sun, E. Gull, and D. Zgid, Relativistic self-consistent GW : Exact two-component formalism with one-electron approximation for solids, *Phys. Rev. B* **106**, 085121 (2022).
- [66] C.-N. Yeh, S. Iskakov, D. Zgid, and E. Gull, Fully self-consistent finite-temperature GW in Gaussian Bloch orbitals for solids, *Phys. Rev. B* **106**, 235104 (2022).
- [67] J. M. Luttinger and J. C. Ward, Ground-State Energy of a Many-Fermion System. II, *Phys. Rev.* **118**, 1417 (1960).
- [68] G. Baym and L. P. Kadanoff, Conservation Laws and Correlation Functions, *Phys. Rev.* **124**, 287 (1961).
- [69] M. J. Hyrkäs, D. Karlsson, and R. v. Leeuwen, Cutting rules and positivity in finite temperature many-body theory, *J. Phys. A: Math. Theor.* **55**, 335301 (2022).
- [70] M. van Schilfgaarde, T. Kotani, and S. Faleev, Quasiparticle Self-Consistent GW Theory, *Phys. Rev. Lett.* **96**, 226402 (2006).
- [71] T. Kotani, M. van Schilfgaarde, and S. V. Faleev, Quasiparticle self-consistent GW method: A basis for the independent-particle approximation, *Phys. Rev. B* **76**, 165106 (2007).
- [72] A. Kutepov, K. Haule, S. Y. Savrasov, and G. Kotliar, Electronic structure of Pu and Am metals by self-consistent relativistic GW method, *Phys. Rev. B* **85**, 155129 (2012).
- [73] A. L. Kutepov, V. S. Oudovenko, and G. Kotliar, Linearized self-consistent quasiparticle GW method: Application to semiconductors and simple metals, *Comput. Phys. Commun.* **219**, 407 (2017).
- [74] F. Kaplan, M. E. Harding, C. Seiler, F. Weigend, F. Evers, and M. J. van Setten, Quasi-Particle Self-Consistent GW for Molecules, *J. Chem. Theory Comput.* **12**, 2528 (2016).
- [75] P. García-González and R. W. Godby, Self-consistent calculation of total energies of the electron gas using many-body perturbation theory, *Phys. Rev. B* **63**, 075112 (2001).
- [76] M. S. Hybertsen and S. G. Louie, Electron correlation in semiconductors and insulators: Band gaps and quasiparticle energies, *Phys. Rev. B* **34**, 5390 (1986).
- [77] H. J. Vidberg and J. W. Serene, Solving the Eliashberg equations by means of N -point Padé approximants, *J Low Temp Phys* **29**, 179 (1977).
- [78] H. Yoon, J.-H. Sim, and M. J. Han, Analytic continuation via domain knowledge free machine learning, *Phys. Rev. B* **98**, 245101 (2018).
- [79] J. Fei, C.-N. Yeh, and E. Gull, Nevanlinna Analytical Continuation, *Phys. Rev. Lett.* **126**, 056402 (2021).
- [80] J. Fei, C.-N. Yeh, D. Zgid, and E. Gull, Analytical continuation of matrix-valued functions: Carathéodory formalism, *Phys. Rev. B* **104**, 165111 (2021).
- [81] Z. Huang, E. Gull, and L. Lin, Robust analytic continuation of Green's functions via projection, pole estimation, and semidefinite relaxation, *Phys. Rev. B* **107**, 075151 (2023).
- [82] A. L. Kutepov, Full versus quasiparticle self-consistency in vertex-corrected GW approaches, *Phys. Rev. B* **105**, 045124 (2022).
- [83] A. L. Kutepov, Self-consistent solution of Hedin's equations: Semiconductors and insulators, *Phys. Rev. B* **95**, 195120 (2017).
- [84] A. Stan, N. E. Dahlen, and R. van Leeuwen, Levels of self-consistency in the GW approximation, *J. Chem. Phys.* **130**, 114105 (2009).
- [85] J. Lei and T. Zhu, Gaussian-based quasiparticle self-consistent GW for periodic systems, *J. Chem. Phys.* **157**, 214114 (2022).
- [86] V. M. Galitskii and A. B. Migdal, Application of quantum field theory methods to the many body problem, *Sov. Phys. JETP* **7**, 18 (1958).
- [87] B. Holm and F. Aryasetiawan, Total energy from the Galitskii-Migdal formula using realistic spectral functions, *Phys. Rev. B* **62**, 4858 (2000).
- [88] G. L. Stoychev, A. A. Auer, and F. Neese, Automatic Generation of Auxiliary Basis Sets, *J. Chem. Theory Comput.* **13**, 554 (2017).
- [89] Q. Sun, T. C. Berkelbach, N. S. Blunt, G. H. Booth, S. Guo, Z. Li, J. Liu, J. D. McClain, E. R. Sayfutyarova, S. Sharma, S. Wouters, and G. K.-L. Chan, PySCF: the Python-based simulations of chemistry framework, *WIREs Comp. Mol. Sci.* **8**, e1340 (2018).
- [90] Q. Sun, X. Zhang, S. Banerjee, P. Bao, M. Barbry, N. S. Blunt, N. A. Bogdanov, G. H. Booth, J. Chen, Z.-H. Cui, J. J. Eriksen, Y. Gao, S. Guo, J. Hermann, M. R. Hermes, K. Koh, P. Koval, S. Lehtola, Z. Li, J. Liu, N. Mardirossian, J. D. McClain, M. Motta, B. Mussard, H. Q. Pham, A. Pulkin, W. Purwanto, P. J. Robinson, E. Ronca, E. R. Sayfutyarova, M. Scheurer, H. F. Schurkus, J. E. T. Smith, C. Sun, S.-N. Sun, S. Upadhyay, L. K. Wagner, X. Wang, A. White, J. D. Whitfield, M. J. Williamson, S. Wouters, J. Yang, J. M. Yu, T. Zhu, T. C. Berkelbach, S. Sharma, A. Y. Sokolov, and G. K.-L. Chan, Recent developments in the PySCF program package, *J. Chem. Phys.* **153**, 024109 (2020).
- [91] J. Li, M. Wallerberger, N. Chikano, C.-N. Yeh, E. Gull, and H. Shinaoka, Sparse sampling approach to efficient ab initio calculations at finite temperature, *Phys. Rev. B* **101**, 035144 (2020).
- [92] H. Shinaoka, N. Chikano, E. Gull, J. Li, T. Nomoto, J. Otsuki, M. Wallerberger, T. Wang, and K. Yoshimi, Efficient ab initio many-body calculations based on sparse modeling of Matsubara Green's function, [arXiv:2106.12685 \[cond-mat, physics:physics\]](https://arxiv.org/abs/2106.12685) (2021).
- [93] J. Paier, R. Hirschl, M. Marsman, and G. Kresse, The Perdew–Burke–Ernzerhof exchange–correlation functional applied to the G2-1 test set using a plane-wave basis set, *J. Chem. Phys.* **122**, 234102 (2005).
- [94] P. Broqvist, A. Alkauskas, and A. Pasquarello, Hybrid-functional calculations with plane-wave basis sets: Effect of singularity correction on total energies, energy eigenvalues, and defect energy levels, *Phys. Rev. B* **80**, 085114 (2009).
- [95] R. Sundararaman and T. A. Arias, Regularization of the Coulomb singularity in exact exchange by Wigner–Seitz truncated interactions: Towards chemical accuracy in nontrivial systems, *Phys. Rev. B* **87**, 165122 (2013).
- [96] S. Choi, P. Semon, B. Kang, A. Kutepov, and G. Kotliar, ComDMFT: A massively parallel computer package for the electronic structure of correlated-electron systems, *Comput. Phys. Commun.* **244**, 277 (2019).
- [97] M. Kaltak, J. Klimeš, and G. Kresse, Low Scaling Algorithms for the Random Phase Approximation:

- Imaginary Time and Laplace Transformations, *J. Chem. Theory Comput.* **10**, 2498 (2014).
- [98] E. Gull, S. Iskakov, I. Krivenko, A. A. Rusakov, and D. Zgid, Chebyshev polynomial representation of imaginary-time response functions, *Phys. Rev. B* **98**, 075127 (2018).
- [99] X. Dong, D. Zgid, E. Gull, and H. U. R. Strand, Legendre-spectral Dyson equation solver with super-exponential convergence, *J. Chem. Phys.* **152**, 134107 (2020).
- [100] J. Kaye, K. Chen, and O. Parcollet, Discrete Lehmann representation of imaginary time Green's functions, *Phys. Rev. B* **105**, 235115 (2022).
- [101] N. Sheng, A. Hampel, S. Beck, O. Parcollet, N. Wentzell, J. Kaye, and K. Chen, Low-rank Green's function representations applied to dynamical mean-field theory, *Phys. Rev. B* **107**, 245123 (2023).
- [102] T. C. Chiang and F. J. Himpsel, *Subvolume A · 2.1.8 BP: Datasheet from Landolt-Börnstein - Group III Condensed Matter · Volume 23A: "Subvolume A" in SpringerMaterials* (1989).
- [103] M. P. Thompson, G. W. Auner, T. S. Zheleva, K. A. Jones, S. J. Simko, and J. N. Hilfiker, Deposition factors and band gap of zinc-blende AlN, *Journal of Applied Physics* **89**, 3331 (2001).
- [104] M. Röppischer, R. Goldhahn, G. Rossbach, P. Schley, C. Cobet, N. Esser, T. Schupp, K. Lischka, and D. J. As, Dielectric function of zinc-blende AlN from 1 to 20 eV: Band gap and van Hove singularities, *J. Appl. Phys.* **106**, 076104 (2009).
- [105] J. S. Kang, M. Li, H. Wu, H. Nguyen, and Y. Hu, Basic physical properties of cubic boron arsenide, *Appl. Phys. Lett.* **115**, 122103 (2019).
- [106] S. Goedecker, M. Teter, and J. Hutter, Separable dual-space Gaussian pseudopotentials, *Phys. Rev. B* **54**, 1703 (1996).
- [107] C. Hartwigsen, S. Goedecker, and J. Hutter, Relativistic separable dual-space Gaussian pseudopotentials from H to Rn, *Phys. Rev. B* **58**, 3641 (1998).
- [108] G. Harsha, V. Abraham, and D. Zgid, Challenges with relativistic GW calculations in solids and molecules, *Faraday Discuss.* [10.1039/D4FD00043A](https://doi.org/10.1039/D4FD00043A) (2024).
- [109] P. Pokhilko, C.-N. Yeh, and D. Zgid, Iterative subspace algorithms for finite-temperature solution of Dyson equation, *J. Chem. Phys.* **156**, 094101 (2022).
- [110] E. McCormack, J. M. Gilligan, C. Cornaggia, and E. E. Eyler, Measurement of high Rydberg states and the ionization potential of h_2 , *Phys. Rev. A* **39**, 2260 (1989).
- [111] Ph. Dugourd, D. Rayane, P. Labastie, B. Vezin, J. Chevalayre, and M. Broyer, Measurements of lithium cluster ionization potentials, *Chem. Phys. Lett.* **197**, 433 (1992).
- [112] T. Trickl, E. F. Cromwell, Y. T. Lee, and A. H. Kung, State-selective ionization of nitrogen in the $x^2\sigma_g^+v_+ = 0$ and $v_+ = 1$ states by two-color (1+1) photon excitation near threshold, *J. Chem. Phys.* **91**, 6006 (1989).
- [113] D. K. Bulgin, J. M. Dyke, and A. Morris, HeI photoelectron spectrum of the $p_2(x^1\sigma_g^+)$ molecule, *J. Chem. Soc., Faraday Trans. 2* **72**, 2225 (1976).
- [114] J. M. Dyke, G. D. Josland, J. G. Snijders, and P. M. Boerrigter, Ionization energies of the diatomic halogens and interhalogens studied with relativistic hartree-fock-slater calculations, *Chem. Phys.* **91**, 419 (1984).
- [115] G. Bieri and L. Åsbrink, 30.4-nm He(II) photoelectron spectra of organic molecules: Part I. Hydrocarbons, *J. Electron Spectrosc. Relat. Phenom* **20**, 149 (1980).
- [116] R. Roberge, C. Sandorfy, J. I. Matthews, and O. P. Strausz, The far ultraviolet and HeI photoelectron spectra of alkyl and fluorine substituted silane derivatives, *J. Chem. Phys.* **69**, 5105 (1978).
- [117] S. G. Lias, R. D. Levin, and S. A. Kafafi, Ion Energetics Data, in *NIST Chemistry WebBook, NIST Standard Reference Database Number 69* (National Institute of Standards and Technology).
- [118] H. Baumgaertel, H. W. Jochims, E. Ruehl, H. Bock, R. Dammel, J. Minkwitz, and R. Nass, Photoelectron spectra and molecular properties. 112. Photoelectron and photoionization mass spectra of the fluoroamines $\text{NH}_3\text{-nFn}$, *Inorg. Chem.* **28**, 943 (1989).
- [119] A. H. Cowley, R. A. Kemp, M. Lattman, and M. L. McKee, Lewis base behavior of methylated and fluorinated phosphines. Photoelectron spectroscopic investigation, *Inorg. Chem.* **21**, 85 (1982).
- [120] G. Bieri, L. Åsbrink, and W. von Niessen, 30.4-nm He (II) photoelectron spectra of organic molecules: Part VII. Miscellaneous compounds, *J. Electron Spectrosc. Relat. Phenom* **27**, 129 (1982).
- [121] M. S. Banna and D. A. Shirley, Molecular photoelectron spectroscopy at 132.3 eV: N_2 , CO , C_2H_4 and O_2 , *J. Electron Spectrosc. Relat. Phenom* **8**, 255 (1976).
- [122] A. W. Potts and W. C. Price, Photoelectron Studies of Ionic Materials using Molecular Beam Techniques, *Phys. Scr.* **16**, 191 (1977).
- [123] J. Kreile, A. Schweig, and W. Theil, Experimental and theoretical investigation of the photoionization of hydrogen cyanide, *Chem. Phys. Lett.* **87**, 473 (1982).
- [124] V. I. Vovna, F. I. Vilesov, and S. N. Lopatin, Photoelectron spectra of hydrazine and some alkyl derivatives, *Opt. Spectrosc.* **38**, 143 (1975).
- [125] A. Vorob'ev, I. Furlei, A. Sultanov, V. Khvostenko, G. Leplyanin, A. Derzhinskii, and G. Tolstikov, Mass spectrometry of resonance capture of electrons and photoelectron spectroscopy of molecules of ethylene oxide, ethylene sulfide, and their derivatives, *Bull. Acad. Sci. USSR, Div. Chem. Sci.*, 1388 (1989).
- [126] F. S. Ashmore and A. R. Burgess, Study of some medium size alcohols and hydroperoxides by photoelectron spectroscopy, *J. Chem. Soc., Faraday Trans. 2* **73**, 1247 (1977).
- [127] K. Kimura, S. Katsumata, Y. Achiba, T. Yamazaki, and S. Iwata, *Handbook of He(I) Photoelectron Spectra of Fundamental Organic Molecules* (Japan Scientific Societies Press, Tokyo, 1981).
- [128] J. H. D. Eland and J. Berkowitz, Photoionization mass spectrometry of HI and DI at high resolution, *J. Chem. Phys.* **67**, 5034 (1977).
- [129] A. W. Potts and T. A. Williams, The observation of "forbidden" transitions in He II photoelectron spectra, *J. Electron Spectrosc. Relat. Phenom* **3**, 3 (1974).
- [130] S. Cradock and R. A. Whiteford, Photoelectron spectra of the methyl, silyl and germyl derivatives of the group VI elements, *J. Chem. Soc., Faraday Trans. 2* **68**, 281 (1972).
- [131] H. Nakasgawa, M. Asano, and K. Kubo, Mass spectrometric study of the vaporization of lithium metasilicate, *J. Nucl. Mater.* **102**, 292 (1981).

- [132] G. H. King, H. W. Kroto, and R. J. Suffolk, The photoelectron spectrum of a short-lived species in the decomposition products of CS₂, *Chem. Phys. Lett.* **13**, 457 (1972).
- [133] D. Colbourne, D. C. Frost, C. A. McDowell, and N. P. C. Westwood, The photoelectron spectra of the isoelectronic molecules hypochlorous acid HOCl and chloramine NH₂Cl, *J. Chem. Phys.* **68**, 3574 (1978).